RESEARCH ARTICLE

Transient fusion ensures granule replenishment to enable repeated release after IgE-mediated mast cell degranulation

Santiago Balseiro-Gomez*, Juan A. Flores*, Jorge Acosta, M. Pilar Ramirez-Ponce and Eva Ales‡

ABSTRACT

To ensure normal immune function, mast cells employ different pathways to release mediators. Here, we report a thus far unknown capacity of mast cells to recycle and reuse secretory granules after an antigen-evoked degranulation process under physiological conditions; this phenomenon involves the existence of a recycling secretory granule pool that is available for release in a short time scale. Rapid endocytic modes contributed to the recycling of ~60% of the total secretory granule population, which involved kiss-and-run and cavicapture mechanisms, causing retention of the intragranular matrix. We found the presence of normal-size granules and giant actomyosin- and dynamin-dependent granules, which were characterized by large quantal content. These large structures allowed the recovered mast cells to release a large amount of 5-HT, compensating for the decrease in the number of exocytosed secretory granules. This work uncovers a new physiological role of the exo–endocytosis cycle in the immunological plasticity of mast cells and reveals a new property of their biological secretion.

KEY WORDS: Kiss-and-run, Cavicapture, Exocytosis, Endocytosis, Proteoglycan, Mast cell

INTRODUCTION

Mast cells are long-lived resident cells that are of great importance in allergic and inflammatory reactions (Abraham and St John, 2010; Galli et al., 2008). When mast cells are stimulated, up to 100% of the granular content can be released within minutes by a process called anaphylactic degranulation, thus enabling a maximal biological effect in its immediate vicinity (Marchand et al., 2003). After degranulation, granules must be recycled in preparation for another round of release. Decades of studies have revealed that secretory cells employ three exocytosis modes (kiss-and-run, full-collapse fusion and compound exocytosis) to control the rate and amount of vesicular content release, thus controlling the potency of exocytic release and mediating exocytosis plasticity – including immunological plasticity (Oskeritzian, 2015). These three exocytosis modes are followed by three endocytosis modes (Wu et al., 2014). During kiss-and-run events, the fusion pore opens and closes, and allows only the release of amines (Alvarez de Toledo et al., 1993; Henkel et al., 2001); a subclass of kiss-and-run is cavicapture (granule cavity capture), where there is a greater expansion of the fusion pore that could allow the release of small proteins (Fulop et al., 2005; Perrais et al., 2004; Taraska et al.,

Departamento Fisiología Médica y Biofísica, Facultad de Medicina, Universidad de 41009 Sevilla, Spain.
*These authors contributed equally to this work

‡Author for correspondence (eales@us.es)

ⓘ E.A., 0000-0002-5536-4616

2003). During kiss-and-run and cavicapture processes, the granule shape remains almost intact, whereas in full-collapse or full-fusion exocytosis, the granule loses its round shape and flattens out in the plane of the plasma membrane, leading to the merging of these two compartments and the complete release of the granule content (Ceridono et al., 2011; Patzak and Winkler, 1986). Full-collapse fusion is followed by classic endocytosis that involves membrane invagination and granule reformation. The third exocytosis mode is compound exocytosis, which involves exocytosis of giant granules that have been pre-formed through granule–granule fusion or through fusion of granules on the already fused but not collapsed granule (Alvarez de Toledo and Fernandez, 1990; Hafez et al., 2003; Scepek and Lindau, 1993). This mode of exocytosis is followed by bulk endocytosis, which retrieves giant granules (Gaffield et al., 2011; Holt et al., 2003; Wu and Wu, 2007).

Mast cells are unique among haematopoietic cells in that they can undergo repeated rounds of degranulation and re-granulation (Burwen, 1982; Dvorak et al., 1987; Kobayasi and Asboe-Hansen, 1969; Slutsky et al., 1987). This capacity of mast cells to release their cellular contents repeatedly is an important feature of these cells in the induction and perpetuation of an allergic or inflammatory reaction. Although the process of recycling of mast cells granules has been morphologically studied (Hammel et al., 1989, 2010), there is no data available showing that internalized membrane can be recycled into new competent secretory granules. Mast cells can recover after IgE-mediated activation and can repeatedly release β-hexosaminidase and express cytokines within a 24-h interval (Xiang et al., 2001). This recycling period is long (hours to days) compared to that of neurons (seconds to minutes) (Alabi and Tsien, 2013). The main difference with synaptic vesicle recycling is that large dense core granules need to be reloaded with matrix proteins to be reused, which most likely involves a re-maturation process involving the Golgi. However, the time for the recovery process is much shorter than that required for granule biogenesis or maturation, which can take several months, as indicated by previous data (Blank et al., 2014; Hammel et al., 2010) showing that mast cells granules are gradually enriched for incoming cargo, such as proteoglycans and proteases, as well as for histamine and serotonin (5-HT). Therefore, the data suggest that mechanisms of granule replenishment after degranulation in mast cells could involve retention of granule shape and proteoglycans, and could be achieved through transient fusion (Williams and Webb, 2000). In this report, we use live-cell imaging to describe the relative contribution of each mode of exo–endocytosis and the mechanisms associated with granule replenishment in mast cells after IgE-mediated degranulation.

RESULTS

Recovery of releasable granules after intense exocytosis

Mast cells that had been previously sensitized with mouse monoclonal IgE against dinitrophenyl (DNP) were stimulated

with the multivalent antigen DNP-conjugated human serum albumin (HSA), which resulted in a typical degranulation response. However, at 24 h after degranulation, mast cells were viable, and they morphologically resembled resting freshly isolated cells (data not shown) (Slutsky et al., 1987). To explore the modes of membrane retrieval and mechanisms of regranulation that allow mast cells to be restored in a relatively short time after degranulation (<24 h), we studied the dynamics of the exo–endocytosis cycle using FM dyes (Cochilla et al., 1999). FM1-43 and similar amphipathic styryl dyes can reversibly stain membranes and are more fluorescent when bound to membranes than when in solution (Cochilla et al., 1999). Here, we used FM fluorescence as an indicator of proper mast cell endocytosis. Cells were stimulated with antigen DNP-conjugated HSA (1 µg/ml) in the presence of FM1-43 (4 µM) dye for 1 h, and after the dye was removed, the cells were incubated for 24 h at 37°C under 5% CO_2 (Fig. 1A). The cells showed a substantial amount of internalized probe (Fig. 1B) as a consequence of a first exo–endocytic process (initial=645±62 a.u.; mean±s.e.m.; Fig. 1D). Many discrete fluorescent spots of different sizes could be detected that probably represented recaptured granules that were stained with FM1-43. After this interval, we stimulated the cells again with Ca^{2+} ionophore A23187 (1 µg/ml) for 3 min. FM de-staining was observed as a consequence of the loss of fluorescence when the recycled granules underwent a new exocytosis event and released their internalized dye (final=229±29 a.u.; Fig. 1B,D; Movie 1). Although antigen-treated cells exhibited a pronounced loss of FM fluorescence (64.55%±3.65; mean± s.e.m.) (Fig. 1E), cells that had been incubated with FM1-43 in the absence of DNP showed limited FM staining (initial=199±28 a.u.; Fig. 1B,D) that barely declined after ionophore application (29.89%±2.97) (Fig. 1C,E; Movie 2). In addition, a distinctive feature of this spontaneous endocytosis was the small size of the fluorescence spots in comparison to those observed in antigen-treated cells (spontaneous, 0.35±0.03 µm²; control, 3.55±0.68 µm²; mean±s.e.m.;

Fig. 1F). These experiments indicated that there was an important fraction of internalized membrane that generated newly releasable granules within 24 h after immunological stimulation.

Recaptured granules can efficiently store and release serotonin

To further demonstrate that recycled granules constitute a pool of mature secretory granules with the capacity to store and release biogenic amines, we combined fluorescence imaging and amperometry. The FM1-43 signal and the electrochemical detection of 5-HT were simultaneously monitored during a second stimulation with A23187 (Fig. 2A,B; Movie 3). There was a close correlation between the time course of fluorescence decay and the cumulative charge of released 5-HT in cells that underwent a second round of degranulation (Fig. 2C), suggesting that most fusion events and detected amperometric spikes result from previously recycled granules. This correlation was not observed in cells that were incubated with FM1-43 dye but had not been previously stimulated (Fig. S1). Analysis of the total number of amperometric spikes per cell showed a reduction in secretory events in cells that underwent a second cycle of exocytosis (second, 53±10 spikes; mean±s.e.m.) compared to that in cells that underwent only their first exocytic response (first, 97±19 spikes) (Fig. 2D). Curiously, the total cumulative charge (Q) was similar between both groups [1178±19 pC (first) vs 1052±136 pC (second); mean±s. e.m.] (Fig. 2E). To explain this conflicting data, we classified spikes into three pools. The first pool, named regular, included spikes up to 10 pC; spikes between 10 and 50 pC constituted the intermediate pool, and last, the pool of giant spikes, incorporated spikes larger than 50 pC. There was no significant difference in the number of spikes per pool between cells that had been stimulated for the first and the second time; however, there was a tendency to find more giant spikes during the last secretory response [0.3%±0.2 (first) vs 4.2±1.6% (second)] (Fig. 2F). In addition, these events had greater
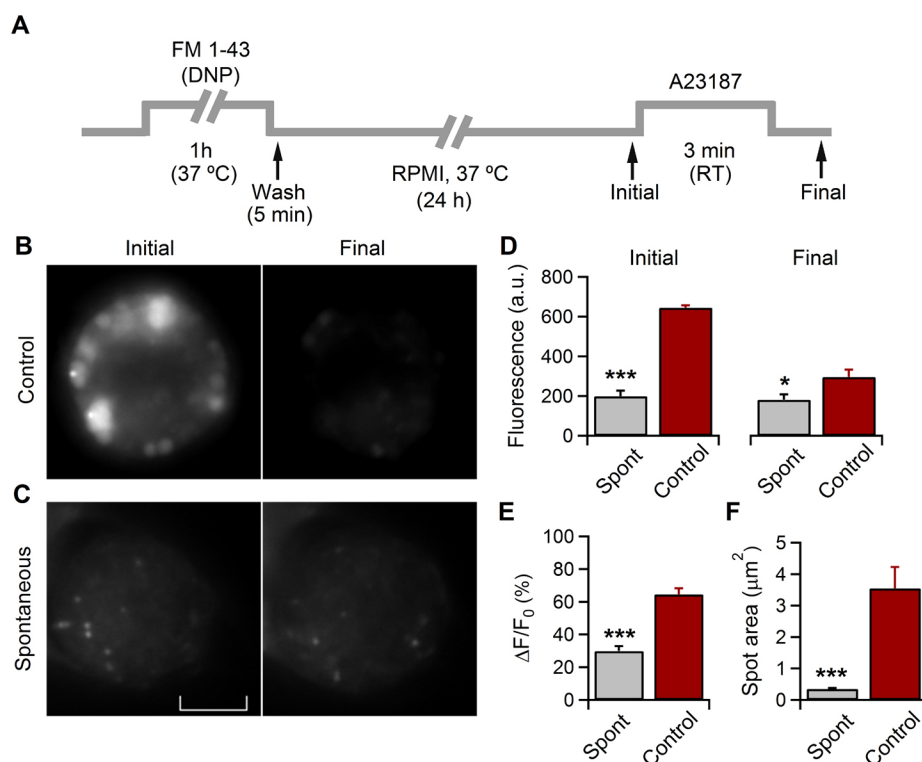

Fig. 1. Evaluation of endocytosis and resultant granule recycling during a single experiment. (A) Experimental scheme explaining the secretory granule labelling assay by measuring the uptake and de-staining of FM1-43 of resting and recovered mast cells cultures. RT, room temperature. (B) Representative images of antigen-stimulated FM-labelled recovered mast cells (Control) before (initial) and after (final) a new degranulation process. (C) Representative images of spontaneous FM1-43 uptake (Spontaneous) before (Initial) and after (Final) a degranulation process. (D) Graphs indicating initial (left) and final (right) values of FM1-43 fluorescence after a second stimulation (A23187). Statistical analysis of fluorescence intensity was performed for both antigen-evoked (Control) and spontaneous (Spont) FM1-43 uptake. (E) Mean fluorescence decrease ($\Delta F/F_0$) for resting (Spont) and recovered (control) mast cells after application of A23187. (F) Plot of the mean area of the endocytic spots observed in resting (Spont) and recovered (Control) mast cells. Error bars are s.e.m.; ***$P<0.001$; *$P<0.050$ by an unpaired two-tailed Student's t-test (D) or Mann–Whitney U test (E,F). Spont, n=10 cells (183 granules); Control n=21 cells (227 granules). Scale bar: 5 µm.
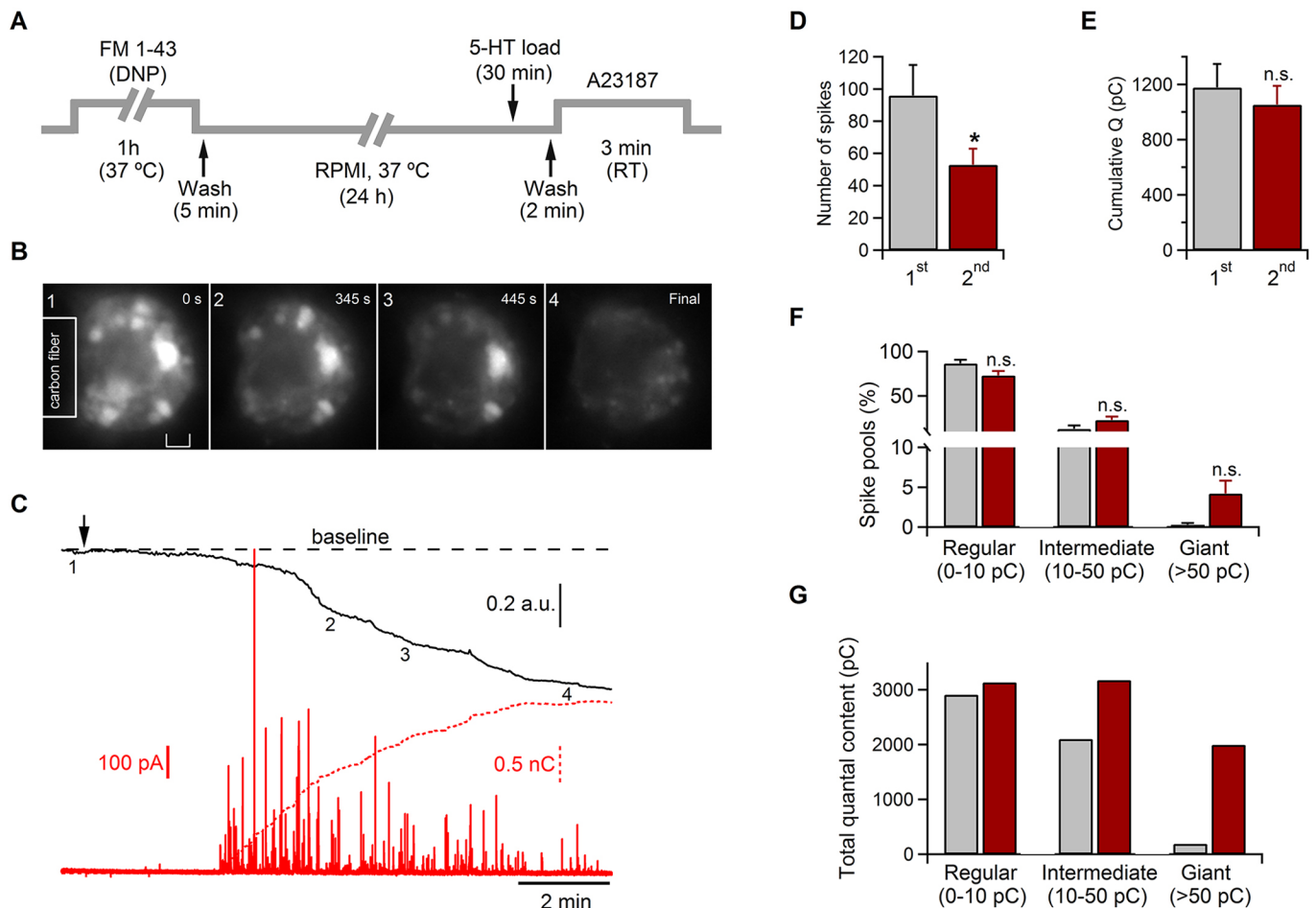
Fig. 2. Recaptured granules can store and release 5-HT. (A) Experimental scheme. RT, room temperature. (B) Movie frames showing a recovered mast cell. Numbers represent images captured at different times during recording. Application of a 3-min 1 µg/ml A23187 stimulus resulted in the progressive loss of bright endocytic spots within the cytoplasm. (C) Traces of the FM1-43 fluorescence time course (black) and amperometric current (red) simultaneously recorded on the mast cells shown in A. Note that the decrease in fluorescence coincided with the liberation of 5-HT (cumulative Q). Numbers indicate when the frames shown in A were captured. (D) Graphs showing the number of spikes pooled from resting (1st) and recovered (2nd) mast cells after application of stimulus (A23187). (E) Graphs showing the average of the total amount of 5-HT released per cell (cumulative Q) that had been stimulated with A23187 for the first time (1st) and after recovery and regranulation (2nd). (F) Spike population, expressed as a percentage of the total spike number and sorted into different quantal content (spike Q), in resting (grey bar) and recovered (red) mast cells that had been stimulated with A23187. (G) Graphs showing the total quantal content for each spike pool in resting (grey bars) and recovered (red bars) mast cells. Error bars are s.e.m.; *$P<0.05$; n.s., not significant, $P \geq 0.050$; an unpaired two-tailed Student's t-test (F, regular spikes) or Mann–Whitney U test (C–F, intermediate and giant spikes). 1st, $n=9$ cells (882 spikes); 2nd $n=16$ cells (1002 spikes). Scale bar: 2 µm (B).

charge (second, $Q=184.15\pm47.12$ pC) and a longer half-width ($t_{1/2}=779.2\pm207.2$ ms; mean±s.e.m.) than their homologues that were obtained during the initial degranulation event (first, $Q=60.48\pm9.22$ pC; $t_{1/2}=127.6\pm54.6$ ms) (Table 1). The representation of total quantal content for each spike pool showed that the giant granules of recovered cells increased total 5-HT release at the expense of decreased total 5-HT release from the reduced number of spikes in the 10–50-pC pool (Fig. 2G).

We concluded that recaptured granules could store and release 5-HT with the same efficacy as unused intact granules and that a low number of large spikes could contribute to compensate for a lower number of fusion events.

Recycling can result in giant secretory granules, which permit the storage of large cargo

When exocytosis occurred at a low frequency, it was easy to correlate each discrete loss of fluorescence that corresponded to a single fusion event with a particular amperometric spike. We observed that fusion of large granules was followed by large spikes (when fusion occurred near the detector) (Fig. 3). For instance, spike 'a' was clearly detected because the granule fused near to the carbon-fibre electrode (CFE), but spike 'b' was poorly recognized because the granule fused far from the detector (Fig. 3A; Movie 4). The second cell showed a more spectacular worm-shaped vacuole; its fusion produced a giant spike with a large half-width ($t_{1/2}=2600$ ms) and charge ($Q=640$ pC) compared with adjacent regular spikes ($t_{1/2}=75.6\pm4.9$ ms, mean±s.e.m.; $Q=3.9\pm 0.2$ pC, mean±s.e.m.) (Fig. 3B; Movie 5). Analysis of the events that fused near to the CFE allowed us to quantify 5-HT content released by endosomes. We classified the events into three groups based on the area of granules (Fig. 3C). First, we observed small spots with a mean size of 1.01 µm² and a spike charge of approximately 8.08 ± 1.5 pC (69%). These fluorescent spots showed an area similar to that of fused regular secretory granules as detected by measuring capacitance (Fernandez et al., 1984). Second, large stained organelles had an average size of 3.3 µm²

Table 1. Amperometric spike pools and secretory parameters in resting and recovered mast cells that were stimulated with A23187

		I_{max} (pA)	$t_{1/2}$ (ms)	Q (pC)	Rise (pA/ms)	Fall (ms)
Regular spikes	1st	56.0±4.6	67.1±3.0	4.0±0.2	4.3±0.8	70.3±2.9
	2nd	48.6±4.0	75.6±4.9	3.9±0.2	3.3±0.5	76.0±4.9
	P-value	0.241**	0.152**	0.897**	0.219*	0.330**
Intermediate spikes	1st	229.3±34.6	75.1±14.7	15.3±1.1	18.0±3.8	75.7±16.8
	2nd	227.3±32.7	141.8±33.1	20.8±1.7	19.9±6.1	121. 2±33.7
	P-value	0.967**	0.214*	0.061*	0.569*	0.383*
Giant spikes	1st	535.4±29.4	127.6±54.6	60.5±9.2	15.5±5.6	71.8±30.6
	2nd	238.1±42.7	779.2±207.2	184.2±47.1	7.9±5.1	532.0±150.4
	P-value	0.001**	0.017**	0.044*	0.178*	0.018**

Parameters of secretory spikes elicited by a 3-min application of A23187 (1 µg/ml) in resting (1st) and recovered (2nd) mast cells. The following parameters were analyzed from the detected spikes: I_{max}, maximum oxidation current; $t_{1/2}$, spike width at half height; spike Q, area of spike or spike net charge; Rise m, ascending slope of spike calculated from 25–75% from I_{max}; fall time, total decay time. Data are presented as mean±s.e.m. The pairs of data sets were compared using a Mann–Whitney U test (*) or a Student's t-test (**). 1st, n=9 cells (882 spikes); 2nd n=16 cells (1002 spikes).

and a mean spike charge of 38.84±8.6 pC (27%). Finally, we defined extra-large endocytic events as those of the cell shown in Fig. 3B, with a mean size of 15.5 µm² and 492.87±76.6 pC of charge (4%). These extensive recycled structures, which probably comprise multiple granules, permit the cells to store a voluminous amount of material without requiring the quantity of membrane necessary to package the same amount of cargo into regular smaller granules. Our calculations indicate that mast cells would have to deplete more than 50 regular granules to release the same amount of 5-HT that a unique large granule can release.

Analysis of single-event fluorescence data showed that de-staining of small spots (area=1.33±0.18 µm², mean±s.e.m.; 31% of total spots) was a fast process (τ=1.39±0.2 s; mean±s.e.m.) compared to the time course of fluorescence decay of large spots (area=3.31±0.69 µm²; 32% of total spots) that decayed more slowly (τ_1=1.53±0.25 s; τ_2=13.10±1.98 s) (where τ_1 is the fast time constant and τ_2 the slow time constant). We found that these large events of slow decay showed a higher amplitude of fluorescence [change in fluorescence (ΔF)=730±85 a.u.] compared to small internalized events that had faster kinetics (ΔF=361±48 a.u.). We also observed that some fraction of fluorescent spots (37%) failed to fuse and to release their dye content (Fig. S2).

Inhibition of dynamin blocks the regranulation of mast cells, and inhibition of actin and myosin II interferes with large granule formation

Roles for actin and dynamin in bulk endocytosis in neurons and neuroendocrine cells have been demonstrated (Dillon and Goda, 2005; Newton et al., 2006; Nguyen et al., 2012). Here, we used the actin polymerization inhibitor cytochalasin D (4 µM) and the dynamin inhibitor dynasore (80 µM) to assess the effect of inhibiting actin and dynamin on the initiation of endocytosis and on the development of large granules and endosomes. In addition, we used blebbistatin (5 µM) to inhibit myosin II, which is also involved in the scission step of endocytosis (Flores et al., 2014). Mast cells were pre-treated with these drugs for 10 min, followed by incubation with FM1-43 and the antigen DNP for 1 h. Preparations were then washed, and internalized fluorescence was visualized (Fig. 4A). Imaging showed that cytochalasin and blebbistatin inhibited ~30% of FM uptake and that dynasore inhibited more than 80% of endocytosis with respect to control cells (Fig. 4B). The area of fluorescent spots from the different conditions was measured, and histograms were created. With respect to control cells (Fig. 4C), the presence of cytochalasin and blebbistatin inhibited the formation of endosomes larger than 2 µm² (mean areas: control=3.55±0.68 µm²,

cytochalasin D=0.87±0.06 µm², blebbistatin=1.06±0.11 µm²; mean±s.e.m.) (Fig. 4D). However, dynasore seems to inhibit all types of endocytosis, except the smallest events, which are likely to correspond with spontaneous events (dynasore=0.67±0.10 µm²) (Fig. 4D).

According to fluorescence imaging, which showed inhibition of large endocytic events after treatment with drugs, amperometric recordings of cells that had been stimulated with a Ca²⁺ ionophore to induce a second round of fusion of releasable granules resulted in a lower number of giant and intermediate spikes and an increase in the number of regular spikes in relation to secretory events detected in control cells (Table S1).

Transient fusion events account for most releasable granules

Next, we conducted experiments to quantify the modes of exocytosis and coupled endocytosis in immunologically stimulated mast cells. Mast cell capacity to undergo different exocytic modes, including full fusion, kiss-and-run transient fusion and compound exocytosis has previously been revealed by using an imaging-based method that uses FITC–dextran (pH sensitive) and Texas-Red–dextran as reporters for granule exocytosis (Cohen et al., 2012). Here, we investigated endocytosis by performing high-resolution confocal imaging of mast cells using FM1-43 dye and fluorescent dextrans of different molecular masses and sizes. pHrodo Green dextran (50 µg/ml) is a 10 kDa dextran–conjugated, pH-sensitive form of Rhodamine that exhibits green fluorescence after endocytosis into the acidic interior of vesicles. pHrodo Green dextran is approximately 5 nm in diameter, whereas FM is ~1 nm (Babich et al., 2008; Wu et al., 2011). FM uptake (in the red channel) might reflect endocytosis of granules through any mechanism and pore size (kiss-and-run, cavicapture, *de novo* endocytosis) (Fig. 5). Because of its smaller size, FM can label recaptured granules created by transient fusion, for instance, that are formed by kiss-and-run. The mean pore diameter, which has been measured during transient fusion events ('capacitance flickers') by analysing fusion-pore conductance in mouse mast cells, is approximately 2 nm (Cabeza et al., 2013). For this reason, the larger pHrodo dye cannot, presumably, enter through a non-expanded fusion pore (<5 nm); therefore, it could not be used to detect kiss-and-run fusion events (Fig. 5A). Our interpretation is that the internalized membrane labelled in red but not in green (probe uptake: 29%±6; labelled granules: 28%±9; mean±s.e.m.) (Fig. 5B,C) should correspond to kiss-and-run events (Fig. 5A; scenario 1). However, the rest of the events in which vesicles were
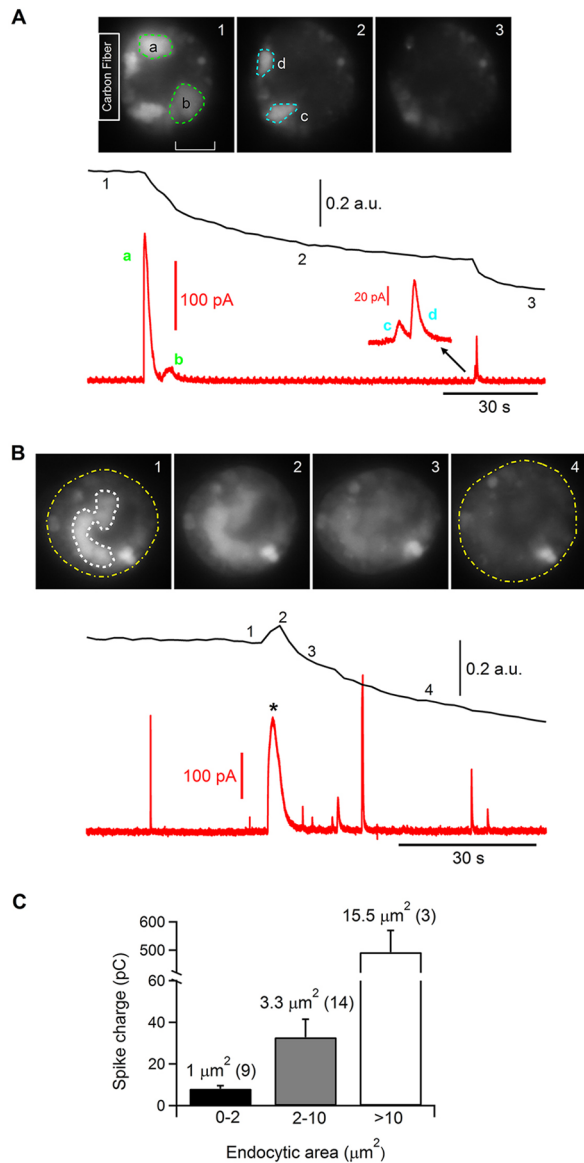
Fig. 3. Evidence of giant secretory granules with large quantal size.
(A) Representative time-lapse imaging frames of FM1-43 de-staining, and traces of the de-staining (black) and amperometric recordings (red) performed simultaneously on a recovered mast cell. Inset shows spikes 'c' and 'd' on expanded amperometric current and time axes. Numbers represent images captured at different times during recording. Note that the closer the CFE was, the better the exocytic event (single spike) could be resolved (dashed lines; spot 'a', area=10.89 μm^2, Q=383 pC; spot 'b', area=13.90 μm^2, Q=44.7 pC; spot c, area=5.48 μm^2, Q=4.21 pC; spot 'd', area=5.36 μm^2, Q=14.4 pC). Note the multigranular morphology of these fluorescent objects, particularly spot 'c' (see also Movie 3).
(B) Representative time-lapse imaging frames of FM1-43 de-staining, and traces of the de-staining (black) and amperometric recordings (red) performed simultaneously on a recovered mast cell. Numbers represent images captured at different times during recording. White dashed line indicates the presence of a worm-shaped endosome (area=21.85 μm^2, Q=640 pC). The change in fluorescence coincided with a giant amperometric spike (black asterisk). Yellow dashed line indicates the cell membrane area before (1) and after fusion of the endosome (4) (Δmembrane area=24.71 μm^2). (C) Charge (Q) of well-resolved spikes plotted against the area of the endocytic spot that evoked the corresponding spike. Numbers above the graphs indicate the mean spot area and number of events recorded in each group. n=9 cells (26 granules: 0–2 μm^2, nine events; 2–10 μm^2, 14 events; >10 μm^2, three events). Numbers in brackets above the bars indicate n values. Error bars are s.e.m. Scale bar: 5 μm.

stained simultaneously in red and green (~71% of probe uptake) (Fig. 5B) were due to the formation of fusion pores larger than 5 nm (Fig. 5A; scenario 2). In addition, to identify endocytosis mediated through cavicapture, which implies the transient formation of an expanded fusion pore, we next combined pHrodo and TRITC–dextran (5 μM) that had a molecular mass of 70 kDa and an estimated diameter of ~12 nm (Babich et al., 2008). This probe (now in the red channel) should stain those internalized granules formed through pores larger than 12 nm. We found that approximately 38%±8 (Fig. 5E) of fluorescence was due to both pHrodo and TRITC–dextran uptake, which corresponded to 55% ±10 of labelled granules (Fig. 5F). In contrast, spots in the green channel but not in the red channel (Fig. 5D; scenario 2) could be interpreted as resulting from cavicapture (5 nm<fusion pore size<12 nm), and spots in both the green and the red channels (Fig. 5D; scenario 1) could also reflect cavicapture endocytosis through an expanded pore larger than 12 nm and/or *de novo* endocytosis. Because heparin proteoglycan, the protein core of the granular matrix, is larger than 700 kDa, it is probable that at least granules internalized through cavicapture and identified by pHrodo labelling retain the proteoglycan matrix in the granular cavity.

In an attempt to define more clearly the recovery process after antigen-mediated degranulation, we used a membrane-impermeable dye, Ruthenium Red (50 $\mu g/ml$) (Fig. S3), which has been shown to have a high affinity for heparin proteoglycan, the main matrix protein in the secretory granules of connective mast cells (Yurt et al., 1977). This staining is irreversible and Ruthenium Red cannot be washed out of the stained cell. The addition of Ruthenium Red to resting mast cells resulted in a complete absence of staining because there were no extruded granules. However, when Ruthenium Red was added to mast cells immediately following their degranulation in response to antigen, nearly all of the cells became intensely stained, as observed by performing differential interference contrast (DIC) microscopy (Fig. S3). In contrast, when Ruthenium Red was added to mast cells 1 h after degranulation, there was little staining. The observed staining was restricted to the cell periphery and extracellular extruded granules but excluded the cell regions labelled with FM1-43, indicating that 1 h after stimulation, granules were internalized, and this rendered them and the secretory granule matrix inaccessible to the dye.

Releasable granules are recovered within a short period
The experiments described above showed that the membrane that is endocytosed after application of antigen is largely recycled to releasable granules. Because kiss-and-run is a very rapid transient fusion mechanism (seconds) and cavicapture reflects a relatively slow mode of kiss-and-run (within seconds to minutes), we determined whether recycled granules are able to undergo a new round of exocytosis immediately after the first hour of initial degranulation with antigen (Fig. 6A). The application of A23187 resulted in apparent FM de-staining and a loss of fluorescent spots, suggesting fusion of recently recaptured granules (Fig. 6B; Movie 6). FM de-staining at 1 h resulted in a 53.70%±3.43 (mean±s.e.m.) fluorescence loss that did not significantly differ from that obtained at 24 h (64.55%±3.65) (Fig. 6C). By contrast, analysis of the total number of amperometric spikes per cell showed a reduction in secretory granules in mast cells after 1 h of recovery respect to mast cells after 24 h of recovery (1 h: regular, 22±5 spikes; intermediate, 1±0.4 spikes; giant, 0.1±0.07 spikes; 24 h: regular, 48±10 spikes; intermediate, 11±3 spikes; giant, 1±0.2 spikes; mean±s.e.m.) (Fig. 6D). Amperometric analysis also showed a lower mean quantal content per spike for the regular pool in mast cells after 1 h
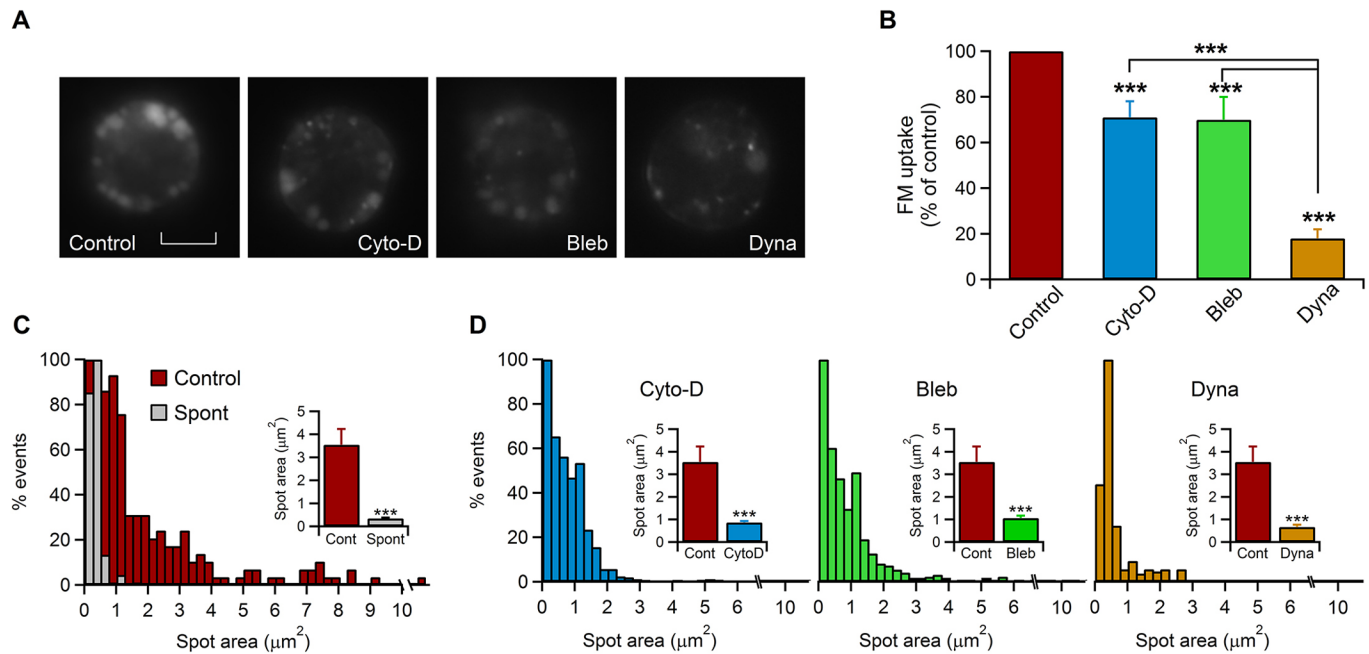
Fig. 4. The effects of dynamin, actin and myosin-II inhibition on granule recycling modes. (A) Representative time-lapse images of FM uptake by mast cells that had been stimulated with antigen (DNP 1 µg/ml) for 1 h in the presence of vehicle (DMSO, 1/1000; Control), cytochalasin D (4 µM; Cyto-D), blebbistatin (5 µM; Bleb) or dynasore (80 µM; Dyna) (see also Table S1). (B) Bars showing the means±s.e.m. of FM uptake expressed relative to control fluorescence, which was set as 100%. Significance, as determined by the Mann–Whitney U test, is shown relative to vehicle-treated cells (Control) and relative to dynasore-treated cells, as indicated. Error bars are s.e.m.; ***$P<0.001$. (C) Distribution of the endocytic spot area (normalized percentage of the total events) in antigen-stimulated cells (Control) and resting cells (Spont, spontaneous). Bin=0.25 µm². (D) Distribution of the endocytic spot area (normalized percentage of the total events) in antigen-stimulated cells in the presence of different drugs: cytochalasin D (4 µM; Cyto-D), blebbistatin (5 µM; Bleb) and dynasore (80 µM; Dyna). Bin=0.25 µm². Inset graphs in C and D show quantification of the mean area of spots formed during endocytic events in control and treated cells. Significance, as determined by the Mann–Whitney U test, is shown relative to vehicle-treated cells (Control). Error bars are s.e.m.; ***$P<0.001$. Spont, $n=12$ cells (183 granules); Control $n=26$ cells (227 granules); Cyto-D, $n=56$ cells (940 granules); Bleb $n=64$ cells (807 granules); Dyna, $n=25$ cells (227 granules). Scale bar: 5 µm.

(2.48±0.20 pC; mean±s.e.m.) than after 24 h of recovery (3.92± 0.24 pC) (Fig. 6E). These data suggest that some steps of granule recondensation and/or maturation are still required to allow the reloading of new 5-HT into recaptured granules.

DISCUSSION

In mast cells, maximal release of 5-HT occurs within the scale of a few minutes, and recycling occurs within the scale of a few hours to days (Blank, 2011). In this study, we found that mechanisms of granule retrieval guarantee the retention of granule shape and proteoglycan matrix (Fig. S4). These mechanisms ensure a fast granule recycling time and a complete capacity to maintain the secretory response during repeated stimulation. This study showed that ~60% of the internalized membrane recycles into new releasable vesicles within 1 h after antigen application, although more time is required to allow the reloading of newly synthesised 5-HT into recaptured granules and to generate fully competent granules (Fig. 6). In fact, 24 h after initial degranulation, despite fewer amperometric spikes, the total release of 5-HT measured during the second round of stimulation was quite similar to the exocytic response measured during initial degranulation (Fig. 2E). Maintenance of the secretory activity through a lower number of fusion events (Fig. 2D) can be achieved with the fusion of only a few additional giant granules, which permit the cells to store and release a large amount of cargo while using less membrane. These events corresponded to ~5% of releasable organelles, which showed a mean area of 15.5 µm² and a mean spike charge of near 500 pC (Fig. 3C). Because a regular granule of approximately 1 µm² might release ~8 pC, these large granules multiply the storage capacity

four times. Therefore, this mode of mast cell recovery efficiently produces secretory organelles to sustain the maximal biological effect under extreme conditions of repeated stimulation.

It is possible that granule aggregates can be formed through transiently fused granules. Granule shapes suggest the fusion of two or more mature granules, which has been previously observed in mast cells (Alvarez de Toledo and Fernandez, 1990; Cabeza et al., 2013). This process has been identified by taking membrane capacitance measurements and could be explained as follows: after sequential fusion of several granules with the plasma membrane, a degranulation sac is formed. This mechanism of exocytosis is called sequential fusion, a subclass of compound exocytosis that has already been described in other secretory cells, such as eosinophils (Hafez et al., 2003) and pancreatic β-cells (Bokvist et al., 2000). If the fusion pore of the first granule that is connected to the plasma membrane is then closed, all the granular cavities are reinternalized as a single unit (Fig. 7). Because FM1-43 might diffuse freely through the interconnected granules, a large structure can be visualized after the fission and removal of extracellular dye. Reloading with 5-HT permits the cell to be ready to release large amounts of transmitter in a new single fusion event. Because endocytosis of large granules, detected by making capacitance measurements (Cabeza et al., 2013), are in the same size range (0–15 µm²) as large organelles visualized by FM1-43, we can rule out that these events are due to multigranular fusion of previously internalized regular granules. In contrast, 48 h after degranulation, fluorescence imaging showed reductions in the number of larger endocytic events and the mean spot area (Fig. S4), suggesting that budding from these composed giant granules occurs gradually, producing smaller granules.
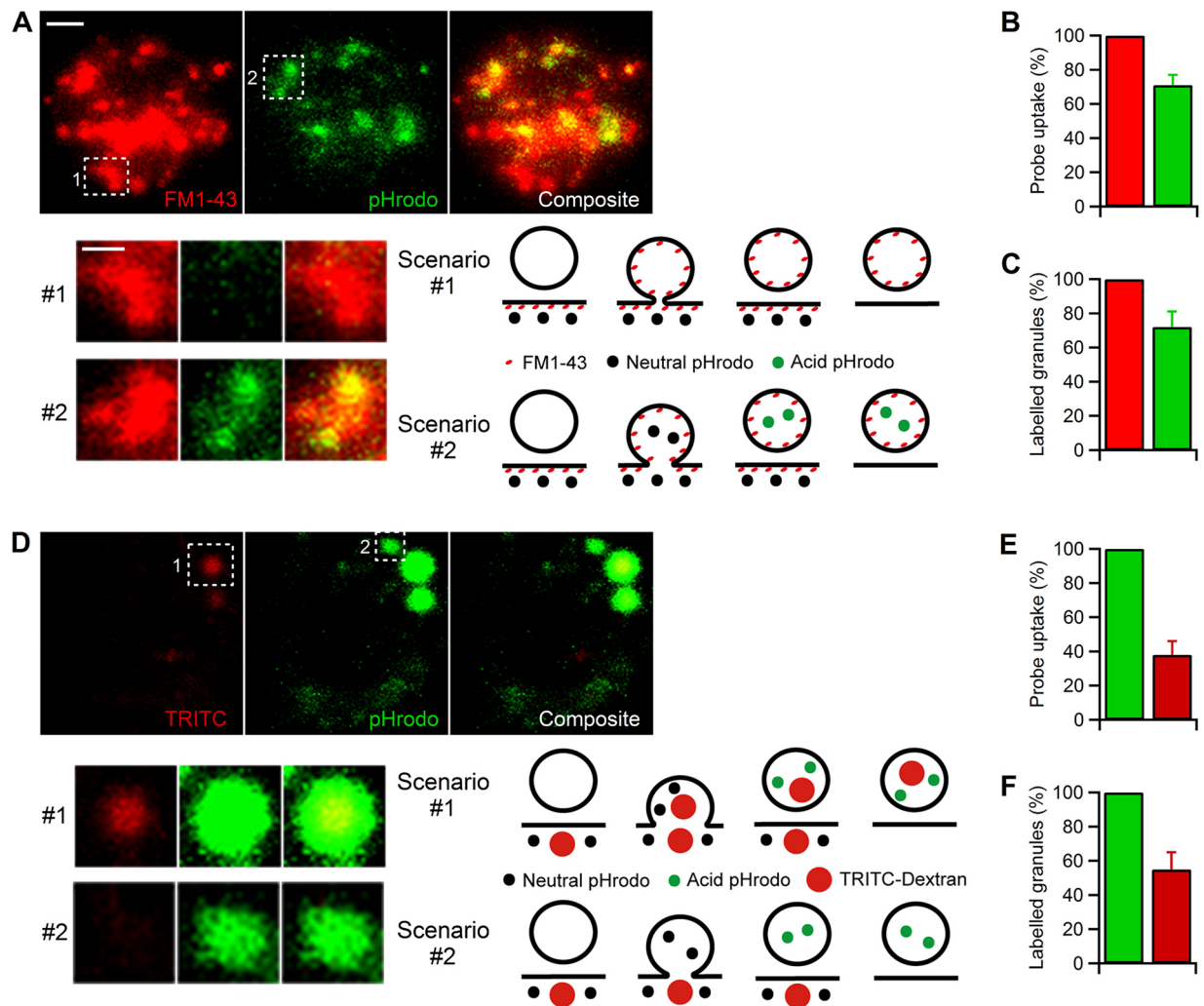
Fig. 5. Evaluation of fusion pore size and endocytic pathways involved in antigen-mediated regranulation. (A) Top, representative confocal images of antigen-stimulated mast cells in the presence of FM1-43 (4 µM) and pHrodo-Green-labelled dextran (50 µg/ml) for 1 h. Bottom right, schematic explaining how some spots in A could stain positively for FM1-43 but negative for pHrodo-Green-labelled dextran (bottom left, zoomed images, scenario 1), and how some spots could stain positively for both dyes (bottom left, zoomed images, scenario 2). Note that the channels were thresholded separately to include all recognizable spots. (B) Graphs showing probe uptake (pHrodo, green) during antigen stimulation relative to uptake of the smaller probe (FM1-43, red). (C) Graphs showing the percentage of granules labelled with pHrodo (green) during antigen stimulation relative those labelled by the smaller probe (FM1-43, red). The percentage of kiss-and-run events (29%±6) is given by the amount of FM-positive and pHrodo-negative granules. (D) Top, representative confocal images of antigen-stimulated (1 h) mast cells in the presence of TRITC–dextran (70 kDa, 5 µM) and pHrodo-Green–dextran (50 µg/ml). Bottom right, schematic explaining how some spots in A could stain positively for both dyes (bottom left, zoomed images, scenario 1) and how some spots could stain positively for pHrodo Green but negative for TRITC (bottom left, zoomed images, scenario 2). (E) Graphs showing probe uptake (TRITC–dextran, red) during antigen stimulation relative to that of the smaller probe (pHrodo Green, green). (F) Graphs showing the percentage of granules labelled with TRITC–dextran (red) during antigen stimulation relative to those labelled by the smaller probe (pHrodo Green, green). The percentage of cavicapture events (32%±8) is given by the number of pHrodo-Green-positive and TRITC-negative granules relative to the percentage of FM-positive and pHrodo-positive granules obtained previously (see also Fig. 7). FM1-43 and pHrodo Green staining, *n*=10 cells; pHrodo Green and TRITC staining, *n*=11 cells. Scale bar: 2 µm (top panels in A,D); 1 µm (zoomed images in A,D).

It is commonly believed that the entire contents of dense-core granules are released on exocytosis. However, existing evidence supports the notion that vesicles might actually release only a portion of these contents (Alés et al., 1999; Artalejo et al., 1998; Bauer et al., 2004a; Taraska et al., 2003) before they are internalized. PC12 cells retain and retrieve their vesicle cores and make them available for subsequent exocytic release within <5 min (Bauer et al., 2004b). In chromaffin cells, one-third of the granules fuse in response to depolarization and reseal within 100 s (Perrais et al., 2004). The recaptured granules can retain vesicle proteins such as chromogranins and tissue plasminogen activator (Fulop et al., 2005; Perrais et al., 2004). Mast cells are characterized by their ability

to selectively release different cargoes in response to different stimuli (Moon et al., 2014). The kiss-and-run mechanism allows the exit of small molecules, such as biogenic amines, but it prevents the release of larger proteins. Fine control of the fusion pore allows the release of some mediators but prevents the escape of others. Our data suggest that approximately 30% of retrieved granules in mast cells use the kiss-and-run mechanism to recycle membrane. This proportion is quite similar to that estimated by using combined cell capacitance and amperometry analyses (Cabeza et al., 2013). During this type of fusion, 5-HT can escape and a slow amperometric signal can be detected (Alvarez de Toledo et al., 1993). The rest of the observed endocytosis
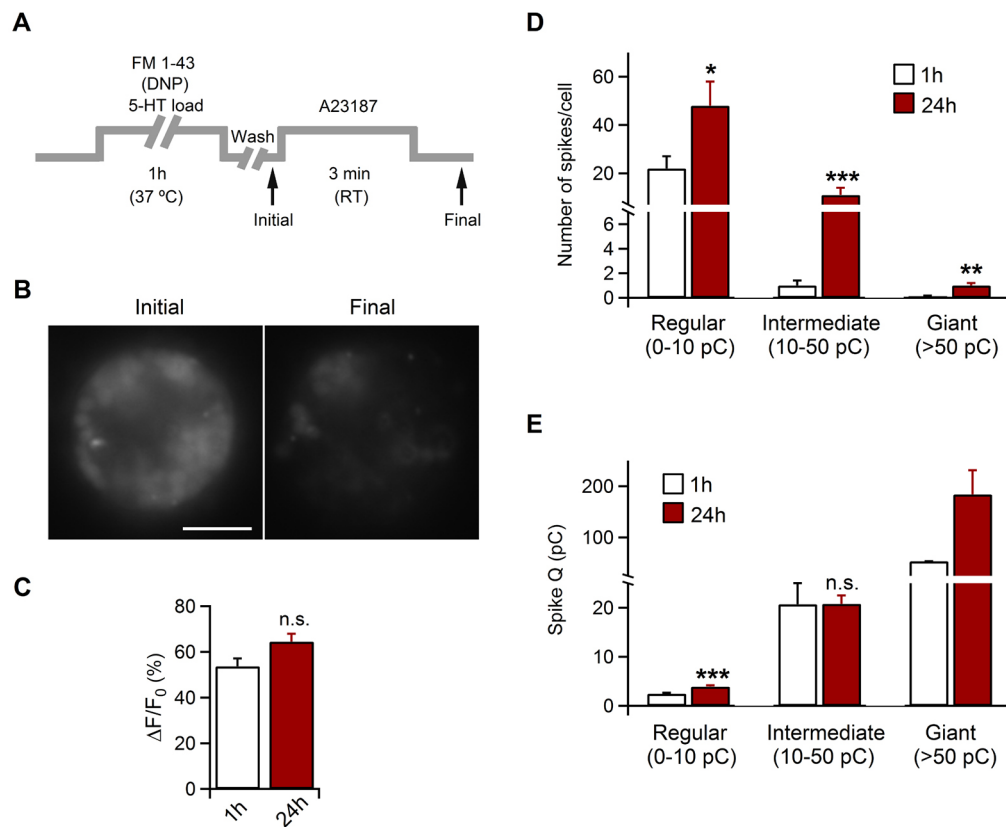
Fig. 6. Releasable granules are rapidly recovered after exocytosis. (A) Experimental scheme for uptake and de-staining of FM1-43. Secretory granules were loaded with FM1-43 (4 µM) and 5-HT (1 mM) for 1 h in the presence of antigen (DNP, 1 µg/ml). The cells were then washed for 5 min, and coverslips with mast cell cultures were transferred to the recording chamber and incubated with basal Locke solution. RT, room temperature. (B) Representative images of recovered mast cells 1 h after antigen stimulation (Initial) and after a second stimulation with A23187 (1 µg/ml) (Final). (C) Graphs showing the magnitude of FM1-43 de-staining ($\Delta F/F_0$) in recovered mast cells after 1 h and 24 h. ΔF: 1 h, $n=14$ cells; 24 h, $n=21$ cells. (D) Graphs showing the number of spikes per cell for each spike pool in recovered mast cells after 1 h and 24 h. (E) Graphs showing spike charge for each spike pool in recovered mast cells after 1 h and 24 h. Error bars are s.e.m.; ***$P<0.001$; **$P<0.01$; *$P<0.05$; n.s., not significant, $P\geq0.050$; unpaired two-tailed Student's t-test (E; regular 0–10 pC) or Mann–Whitney U test (C–E). There were no significant differences between 1 h and 24 h in intermediate and giant spikes. ΔF in C: 1 h, $n=14$ cells; 24 h, $n=21$ cells. Amperometry in D,E: 1 h, $n=15$ cells (346 spikes); 24 h, $n=16$ cells (1002 spikes). Scale bar: 5 µm.

might occur through a coupling mechanism that requires the expansion of a fusion pore larger than 5 nm, allowing pHrodo entry and staining of fused granules in green. If the fusion pore closes, a transient fusion event through a dilated pore occurs. This mode of exo–endocytosis, which still preserves granule shape, is called cavicapture and seems to account for another 30% of internalized granules (Fig. 5). Through a fusion pore of this size, complete 5-HT content and small proteins can escape, such as proteases and peptides (Perrais et al., 2004). However, the indissoluble core matrix of proteoglycan is likely to be retained in the granule cavity because of its high molecular mass (700–900 kDa). In fact, our results with Ruthenium Red dye suggest that an early step after immunological degranulation is the closure of fused granules, thereby preventing the escape of this large material and their staining with dye when this is added 1 h after degranulation. Therefore, granules retrieved through rapid endocytosis (kiss-and-run and cavicapture) maintain their membrane shape and functionality. Repeated stimulation of mast cells mobilizes a pool of releasable granules that are likely to selectively release their contents through a transient fusion pore. These renewed granules are almost instantly available for re-use, that is, these granules must be refilled while they are attached to the plasma membrane.

The rest of the reinternalized granules (40%) were captured through a pore larger than 12 nm (Fig. 7); however, we do not know

which endocytic mechanism operates here – i.e. cavicapture, which involves a larger expanded fusion pore that allows TRITC–dextran entry, or *de novo* endocytosis, where a plasma membrane piece is invaginated and retrieved. Because fluorescent spots stained with pHrodo showed a larger diameter (1.63±0.25 µm²; mean±s.e.m.) than the same spots stained with TRITC–dextran (1.39±0.17 µm²) (Fig. 5), it is probable that the fusion pore could still restrict the access of the larger dye to the granule cavity. In that case, cavicapture should be the most probable mechanism. Regardless, it is possible that proteoglycans and large molecules can escape through a pore of larger dimensions. In that case, it is rational that a longer period of recycling through the trans-Golgi network is required to form part of a new granule. This fraction of granules identified by TRITC–dextran labelling is quantitatively similar to the fraction of fluorescent spots that failed to undergo a second round of exocytosis (Fig. S2).

It has been proposed that the GTPase dynamin promotes the closure of an already expanded fusion pore. This idea is supported by the fact that the disruption of dynamin GTPase activity increases the quantal size (Elhamdani et al., 2001; González-Jamett et al., 2010, 2013; Graham et al., 2002) and hinders the rapid reuptake (cavicapture) of secretory vesicles (Holroyd et al., 2002; Tsuboi et al., 2004). Here, we demonstrate that the recapture of large dense-core granules in mast cells is mediated by dynamin. Dynasore
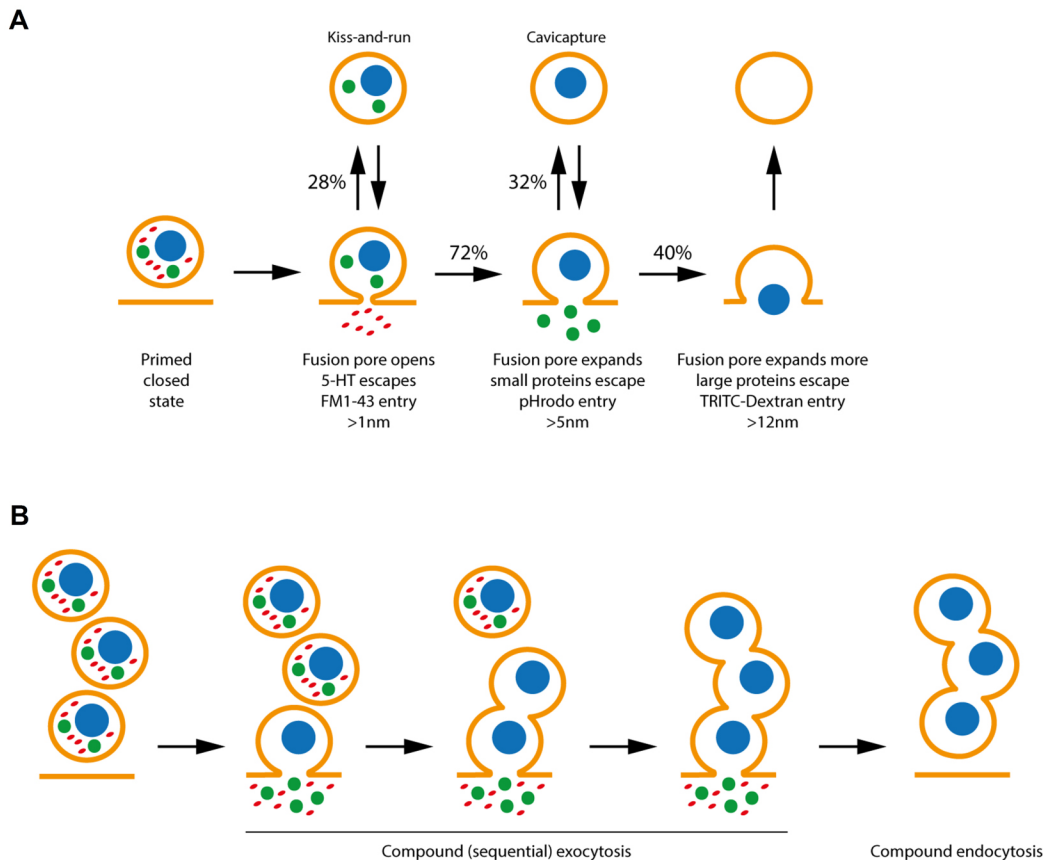
Fig. 7. A schematic summarizing exo–endocytosis events during antigen stimulation in mast cells. (A) A diagram illustrating the different exo–endocytic routes operating during antigen stimulation in mast cells (see also Fig. 5). (B) A diagram illustrating the compound exo–endocytic mechanism that secretory granules undergo during antigen stimulation in mast cells.

inhibited all forms of IgE-mediated endocytosis (Fig. 4), thus indicating a dynamin-dependent reclosure of exocytic fusion pore during kiss-and-run and cavicapture events. Cytochalasin D and blebbistatin inhibited release of most of the larger granules. Because these events seem to be the result of multivesicular structures that disconnected from the plasma membrane through a transient fusion pore, it is unlikely that a complex of actomyosin might be required to mediate the closure of a fusion pore after a multigranular fusion event but not after a single-granular fusion event. The actomyosin complex is likely to play a role in establishing granule–granule contact during sequential fusion. It is possible that inhibition of myosin II and of actin polymerization might preclude sequential fusion of granules but allow fusion and subsequent closure of primary secretory granules that are in contact with the plasma membrane, resulting in a small secretory response. In fact, the second round of stimulation in cells that had been pretreated with inhibitors produced amperometric spikes of smaller amplitude and charge, and reduced the number of giant spikes (Table S1).

The finding that mast cells can undergo a process of rapid restoration and regranulation is a fundamental biological event. We used A23187 instead of immunological stimulation to mediate a second round of exocytosis because peritoneal mast cells have been proven to undergo a period of unresponsiveness to immunologic reactivation (data not shown; Levi-Schaffer et al., 1990). Therefore, it is possible that after IgE-dependent activation, mast cells exhibit a state of physiologic desensitization to a subsequent immunologic stimulation event. However, in addition to allergic triggers, mast cells can be activated by anaphylatoxins, antibody light chains, cytokines

and neuropeptides. Increasing evidence also indicates that mast cell dysfunction underlies many common inflammatory disorders (Bischoff, 2016; Metz et al., 2007; Mican and Metcalfe, 1990; Pedotti et al., 2003), where mast cells show a hyper-activated phenotype. Here, we elucidated that kiss-and-run and cavicapture are the dominant mechanisms that mediate the rapid reuse of secretory granules after IgE-mediated activation. This capacity to undergo continuous cycles of degranulation and regranulation could support the aberrant and potentially detrimental role of mast cells in chronic inflammatory diseases. Therefore, increasing our knowledge of the molecules and mechanisms involved in mediating exo- and endocytosis in response to specific stimuli will provide opportunities to develop novel therapeutic targets for the treatments of increasingly wide-spread allergic and other inflammatory diseases.

MATERIALS AND METHODS
All research involving animals was performed following a protocol approved by the Ethical Committee of the University of Seville and Consejería de Agricultura y Pesca (Junta de Andalucía, Spain) in accordance with the European Communities Council Directive 86/609/ZZC and with the Spanish Royal Decree RD 1201/2005. All efforts were made to minimize the number of animals used and their suffering. All animals were euthanized with CO_2.

Animals, mast cell culture and secretory granule labelling assay
Mast cells were obtained from 4- to 5-month-old wild-type C57BL/6 mice. Both male and female mice were used for the experiments. Fully differentiated peritoneal mast cells cultures were prepared according to a previously published protocol with minor modifications (Kovarova, 2013). Mast cells were plated at a density of 10×10^3–15×10^3 cells/well. Cultures

were maintained in glutamine (4 mM) and FBS (5% v/v) (BioWest) Advanced RPMI 1640 medium (Gibco) containing penicillin (50 U/ml) and streptomycin (50 μg/ml) (Gibco), stem cell factor (30 ng/ml) and IL-3 (10 ng/ml) (PeproTech) at 37°C under a 5% CO_2 humidified atmosphere. To induce antigen stimulation, mast cells were sensitized with mouse monoclonal anti-DNP IgE (1 μg/ml) (Sigma) in medium for 24 h (Balseiro-Gomez et al., 2015).

For FM1-43 (Invitrogen) loading through spontaneous activity, mast cells were incubated in FM1-43 (4 μM) in basal Locke solution for 60 min (at 37°C under a 5% CO_2 humidified atmosphere). For FM1-43 loading through antigen stimulation, mast cells were incubated in FM1-43 in basal Locke solution containing DNP-conjugated human serum albumin (1 μg/ml) (Sigma) for 60 min. To analyse the roles of actomyosin-II and dynamin in the secretory granule recycling process, cultured mast cells were first preincubated in basal Locke solution supplemented with cytochalasin D (4 μM), blebbistatin (5 μM), dynasore (80 μM) or vehicle (DMSO, 1:1000) (Sigma) in the absence of DNP for 10 min, after which the cells were incubated in FM1-43 in basal Locke solution containing DNP and the different drugs for 60 min. The cells were then washed for 5 min, and coverslips with mast cell cultures were transferred to RPMI medium. The basal Locke solution contained 140 mM NaCl, 10 mM HEPES, 3 mM KOH, 2 mM $CaCl_2$, 1 mM $MgCl_2$ and 10 mM glucose. The pH of the solution was adjusted to 7.3 with NaOH. All chemicals were purchased from Sigma.

Time-lapse and FM dye imaging, and analysis

For time-lapse imaging of recycled secretory granule release, mast cells were treated as described above and imaged 24 h later. Images were obtained using a 63× PlanNeofluar (NA 1.3) oil immersion lens (Zeiss) on an Axiovert 200 inverted microscope equipped with a standard filter set for FM1-43 dye (XF115-2; Omega Optical). Images were captured with an ORCA-R^2 CCD camera (Hamamatsu Photonics) controlled by HCImage software (Hamamatsu Photonics). Time-lapse images were acquired at a rate of 0.5 Hz, 1344×1024 pixels (binned 1×1), with an exposure time of 200 ms. Recovered mast cell de-staining experiments were performed by stimulating cells for 3 min with a Ca^{2+} ionophore (A23187 1 μg/ml; Sigma).

To measure FM unloading, time-lapse recordings were loaded into HCImage software. Responding mast cells (or secretory granules) were manually selected as regions of interest (ROI), and background signals were measured from ROIs placed immediately surrounding the cells. Raw de-staining trace values were extracted and loaded into Excel (Microsoft) and Igor Pro (Wavemetrics) for further analysis. Before normalization, all raw de-staining traces were background corrected using the following formula: F(t) =F_{raw}(t)−F_b(t), where F_{raw}(t) and F_b(t) are the intensity of a raw trace and the corresponding background trace, respectively, at time t. The corrected traces were graphed as the change in fluorescence (ΔF, absolute values) normalized to the fluorescence at the beginning of the experiment (F_0) using the following equation: $\Delta F/F_0 = (F_F - F_0)/F_0$, where F_F is the point at which the de-staining curve slope becomes zero. To measure the fluorescent endocytic secretory granule area, we performed a frame-by-frame analysis of each cell. Spots were manually selected and duplicated, and those that were not well-limited were discarded. Single secretory granule release events were defined by either a single exponential decay to final fluorescence (fast-decaying events) or a double exponential decay (slow-decaying events). Some fraction of the total events showed no change in fluorescence (failure events).

In addition, brightness and contrast were often enhanced to enable easier visualization of FM1-43 labelling. Therefore, the original image resolution was not always apparent from the images shown. Data analysis was always performed on raw images. All experiments were performed at room temperature (22–25°C). Experiments were performed alternating between those with treated cells and control cells.

Amperometry recording and analysis

Ca^{2+}-triggered exocytosis of mast cell granules was monitored by placing a CFE near the cell. Detection of 5-HT release from secretory granules was performed as previously described elsewhere (Alvarez de Toledo et al., 1993; Balseiro-Gomez et al., 2015). Before amperometry recording, cells were incubated in basal Locke solution containing 5-HT (1 mM) for 30 min at 37°C. Then, cells were washed for 2 min, and coverslips were transferred

to a recording chamber with 5-HT-free Locke solution. For experiments shown in Fig. 6, cells were incubated in FM1-43 in basal Locke solution containing DNP-conjugated human serum albumin and 5-HT for 60 min at 37°C. We found no significant differences between 5-HT-loaded control cells of different protocols (5-HT loading time) (data not shown). Off-line analysis was performed using an automated macro written in Igor (Mosharov and Sulzer, 2005). For each cell, we examined only well-resolved spikes with amplitudes >10 pA, and all events were inspected to avoid false-positive events. The amperometric integral (cumulative Q) was calculated by subtracting the constant direct current level in the CFE and integrating the whole amperometric recording.

Confocal microscopy and image analysis

We designed an optical assay to measure the dilation of fusion–fission pores during antigen stimulation based on the size exclusion of different fluorescent markers (Flores et al., 2014) (see Results) – FM1-43 (4 μM), pHrodo-Green-labelled dextran (50 μg/ml; Invitrogen) and 70-kDa-dextran conjugated to TRITC dye (5 μM; Sigma). For probe loading through antigen stimulation, mast cells were incubated in basal Locke solution containing DNP (1 μg/ml) and the different probes for 60 min (at 37°C under a 5% CO_2 humidified atmosphere).

Live-cell confocal images were acquired on an Olympus FV1000 upright confocal microscope with a 60× (NA 1.1) water-immersion lens. During image acquisition, an alternating sequence of laser pulses was used to illuminate labelled spots (laser pulse at a 561-nm wavelength for both FM1-43 and TRITC, and a 488-nm wavelength for pHrodo Green). Fluorescence was filtered at 580–620 nm (FM1-43), 570–600 nm (TRITC) or 500–560 nm (pHrodo Green) according to their emission wavelengths. Images were acquired with identical laser and gain settings. Channels were thresholded separately to include all recognizable spots.

Using ImageJ software (National Institutes of Health), each slice from the 1 μm z-stack was projected (maximal intensity projection). To obtain a population of spots that were as representative as possible of the different endocytic events, pixel quantification was performed with HCImage software in the following manner: a fluorescence intensity threshold was set using a method that included pixels with values above a certain level and excluded the pixels with low values (dark pixels). After the automatic detection of all events, a series of binary operations was applied to the image binary overlay (prune, break nodes, fill holes and separator). Finally, images were filtered in regards to a minimal area for each cell. We determined the percentage of larger probe uptake by subtracting the total area of one channel (larger probe signal) from the corresponding channel (smaller probe signal). As we observed differences in spot size, to avoid a bias caused by these differences, we performed z scans for each channel. We always selected the plane of best focus and a single endocytic event for each cell. The percentage of labelled granules was determined as the percentage of the total area labelled by the probe divided by the corresponding mean area resulting from a single event.

Statistical analysis

Differences between groups were tested for statistical significance using Student's t-test for unpaired data when the data passed a normality test (Lilliefors corrected Kolmogorov–Smirnov) and a Mann–Whitney U test when it did not (Ghasemi and Zahediasl, 2012). The data were regarded as statistically different when $P<0.05$. All statistical analyses were performed using SPSS Statistics 22 software (IBM). All data are plotted as the mean± s.e.m. The presented data represent experiments performed with mast cells from at least three different cultures.

Author contributions
E.A., J.A.F. and S.B.-G. designed the experiments. E.A., J.A.F., S.B.-G., M.P.R.-P. and J.A. performed the experiments. E.A. and S.B.-G. wrote the manuscript. All authors discussed the results and commented on the manuscript.

References

Abraham, S. N. and St John, A. L. (2010). Mast cell-orchestrated immunity to pathogens. *Nat. Rev. Immunol.* **10**, 440-452.

Alabi, A. A. and Tsien, R. W. (2013). Perspectives on kiss-and-run: role in exocytosis, endocytosis, and neurotransmission. *Annu. Rev. Physiol.* **75**, 393-422.

Alés, E., Tabares, L., Poyato, J. M., Valero, V., Lindau, M. and Alvarez de Toledo, G. (1999). High calcium concentrations shift the mode of exocytosis to the kiss-and-run mechanism. *Nat. Cell Biol.* **1**, 40-44.

Alvarez de Toledo, G. and Fernandez, J. M. (1990). Compound versus multigranular exocytosis in peritoneal mast cells. *J. Gen. Physiol.* **95**, 397-409.

Alvarez de Toledo, G., Fernández-Chacón, R. and Fernández, J. M. (1993). Release of secretory products during transient vesicle fusion. *Nature* **363**, 554-558.

Artalejo, C. R., Elhamdani, A. and Palfrey, H. C. (1998). Secretion: dense-core vesicles can kiss-and-run too. *Curr. Biol.* **8**, R62-R65.

Babich, V., Meli, A., Knipe, L., Dempster, J. E., Skehel, P., Hannah, M. J. and Carter, T. (2008). Selective release of molecules from Weibel-Palade bodies during a lingering kiss. *Blood* **111**, 5282-5290.

Balseiro-Gomez, S., Flores, J. A., Acosta, J., Ramirez-Ponce, M. P. and Ales, E. (2015). Identification of a new exo-endocytic mechanism triggered by corticotropin-releasing hormone in mast cells. *J. Immunol.* **195**, 2046-2056.

Bauer, R. A., Overlease, R. L., Lieber, J. L. and Angleson, J. K. (2004a). Retention and stimulus-dependent recycling of dense core vesicle content in neuroendocrine cells. *J. Cell Sci.* **117**, 2193-2202.

Bauer, R. A., Khera, R. S., Lieber, J. L. and Angleson, J. K. (2004b). Recycling of intact dense core vesicles in neurites of NGF-treated PC12 cells. *FEBS Lett.* **571**, 107-111.

Bischoff, S. C. (2016). Mast cells in gastrointestinal disorders. *Eur. J. Pharmacol.* **778**, 139-145.

Blank, U. (2011). The mechanisms of exocytosis in mast cells. *Adv. Exp. Med. Biol.* **716**, 107-122.

Blank, U., Madera-Salcedo, I. K., Danelli, L., Claver, J., Tiwari, N., Sánchez-Miranda, E., Vázquez-Victorio, G., Ramírez-Valadez, K. A., Macias-Silva, M. and González-Espinosa, C. (2014). Vesicular trafficking and signaling for cytokine and chemokine secretion in mast cells. *Front. Immunol.* **5**, 453.

Bokvist, K., Holmqvist, M., Gromada, J. and Rorsman, P. (2000). Compound exocytosis in voltage-clamped mouse pancreatic beta-cells revealed by carbon fibre amperometry. *Pflügers Arch. Eur. J. Physiol.* **439**, 634-645.

Burwen, S. J. (1982). Recycling of mast cells following degranulation in vitro: an ultrastructural study. *Tissue Cell* **14**, 125-134.

Cabeza, J. M., Acosta, J. and Alés, E. (2013). Mechanisms of granule membrane recapture following exocytosis in intact mast cells. *J. Biol. Chem.* **288**, 20293-20305.

Ceridono, M., Ory, S., Momboisse, F., Chasserot-Golaz, S., Houy, S., Calco, V., Haeberlé, A.-M., Demais, V., Bailly, Y., Bader, M.-F. et al. (2011). Selective recapture of secretory granule components after full collapse exocytosis in neuroendocrine chromaffin cells. *Traffic* **12**, 72-88.

Cochilla, A. J., Angleson, J. K. and Betz, W. J. (1999). Monitoring secretory membrane with FM1-43 fluorescence. *Annu. Rev. Neurosci.* **22**, 1-10.

Cohen, R., Corwith, K., Holowka, D. and Baird, B. (2012). Spatiotemporal resolution of mast cell granule exocytosis reveals correlation with Ca2+ wave initiation. *J. Cell Sci.* **125**, 2986-2994.

Dillon, C. and Goda, Y. (2005). The actin cytoskeleton: integrating form and function at the synapse. *Annu. Rev. Neurosci.* **28**, 25-55.

Dvorak, A. M., Schleimer, R. P. and Lichtenstein, L. M. (1987). Morphologic mast cell cycles. *Cell. Immunol.* **105**, 199-204.

Elhamdani, A., Palfrey, H. C. and Artalejo, C. R. (2001). Quantal size is dependent on stimulation frequency and calcium entry in calf chromaffin cells. *Neuron* **31**, 819-830.

Fernandez, J. M., Neher, E. and Gomperts, B. D. (1984). Capacitance measurements reveal stepwise fusion events in degranulating mast cells. *Nature* **312**, 453-455.

Flores, J. A., Balseiro-Gomez, S., Cabeza, J. M., Acosta, J., Ramirez-Ponce, P. and Ales, E. (2014). A new role for myosin II in vesicle fission. *PLoS ONE* **9**, e100757.

Fulop, T., Radabaugh, S. and Smith, C. (2005). Activity-dependent differential transmitter release in mouse adrenal chromaffin cells. *J. Neurosci.* **25**, 7324-7332.

Gaffield, M. A., Romberg, C. F. and Betz, W. J. (2011). Live imaging of bulk endocytosis in frog motor nerve terminals using FM dyes. *J. Neurophysiol.* **106**, 599-607.

Galli, S. J., Tsai, M. and Piliponsky, A. M. (2008). The development of allergic inflammation. *Nature* **454**, 445-454.

Ghasemi, A. and Zahediasl, S. (2012). Normality tests for statistical analysis: a guide for non-statisticians. *Int. J. Endocrinol. Metab.* **10**, 486-489.

González-Jamett, A. M., Báez-Matus, X., Hevia, M. A., Guerra, M. J., Olivares, M. J., Martínez, A. D., Neely, A. and Cárdenas, A. M. (2010). The association of dynamin with synaptophysin regulates quantal size and duration of exocytotic events in chromaffin cells. *J. Neurosci.* **30**, 10683-10691.

González-Jamett, A. M., Momboisse, F., Guerra, M. J., Ory, S., Báez-Matus, X., Barraza, N., Calco, V., Houy, S., Couve, E., Neely, A. et al. (2013). Dynamin-2 regulates fusion pore expansion and quantal release through a mechanism that involves actin dynamics in neuroendocrine chromaffin cells. *PLoS ONE* **8**, e70638.

Graham, M. E., O'Callaghan, D. W., McMahon, H. T. and Burgoyne, R. D. (2002). Dynamin-dependent and dynamin-independent processes contribute to the regulation of single vesicle release kinetics and quantal size. *Proc. Natl. Acad. Sci. USA* **99**, 7124-7129.

Hafez, I., Stolpe, A. and Lindau, M. (2003). Compound exocytosis and cumulative fusion in eosinophils. *J. Biol. Chem.* **278**, 44921-44928.

Hammel, I., Lagunoff, D. and Krüger, P.-G. (1989). Recovery of rat mast cells after secretion: a morphometric study. *Exp. Cell Res.* **184**, 518-523.

Hammel, I., Lagunoff, D. and Galli, S. J. (2010). Regulation of secretory granule size by the precise generation and fusion of unit granules. *J. Cell. Mol. Med.* **14**, 1904-1916.

Henkel, A. W., Kang, G. and Kornhuber, J. (2001). A common molecular machinery for exocytosis and the "kiss-and-run" mechanism in chromaffin cells is controlled by phosphorylation. *J. Cell Sci.* **114**, 4613-4620.

Holroyd, P., Lang, T., Wenzel, D., De Camilli, P. and Jahn, R. (2002). Imaging direct, dynamin-dependent recapture of fusing secretory granules on plasma membrane lawns from PC12 cells. *Proc. Natl. Acad. Sci. USA* **99**, 16806-16811.

Holt, M., Cooke, A., Wu, M. M. and Lagnado, L. (2003). Bulk membrane retrieval in the synaptic terminal of retinal bipolar cells. *J. Neurosci.* **23**, 1329-1339.

Kobayasi, T. and Asboe-Hansen, G. (1969). Degranulation and regranulation of human mast cells. An electron microscopic study of the whealing reaction in urticaria pigmentosa. *Acta Derm. Venereol.* **49**, 369-381.

Kovarova, M. (2013). Isolation and characterization of mast cells in mouse models of allergic diseases. *Methods Mol. Biol.* **1032**, 109-119.

Levi-Schaffer, F., Gare, M. and Shalit, M. (1990). Unresponsiveness of rat peritoneal mast cells to immunologic reactivation. *J. Immunol.* **145**, 3418-3424.

Marchand, F., Mecheri, S., Guilloux, L., Iannascoli, B., Weyer, A. and Blank, U. (2003). Human serum IgE-mediated mast cell degranulation shows poor correlation to allergen-specific IgE content. *Allergy* **58**, 1037-1043.

Metz, M., Grimbaldeston, M. A., Nakae, S., Piliponsky, A. M., Tsai, M. and Galli, S. J. (2007). Mast cells in the promotion and limitation of chronic inflammation. *Immunol. Rev.* **217**, 304-328.

Mican, J. M. and Metcalfe, D. D. (1990). Arthritis and mast cell activation. *J. Allergy Clin. Immunol.* **86**, 677-683.

Moon, T. C., Befus, A. D. and Kulka, M. (2014). Mast cell mediators: their differential release and the secretory pathways involved. *Front. Immunol.* **5**, 569.

Mosharov, E. V. and Sulzer, D. (2005). Analysis of exocytotic events recorded by amperometry. *Nat. Methods* **2**, 651-658.

Newton, A. J., Kirchhausen, T. and Murthy, V. N. (2006). Inhibition of dynamin completely blocks compensatory synaptic vesicle endocytosis. *Proc. Natl. Acad. Sci. USA* **103**, 17955-17960.

Nguyen, T. H., Maucort, G., Sullivan, R. K. P., Schenning, M., Lavidis, N. A., McCluskey, A., Robinson, P. J. and Meunier, F. A. (2012). Actin- and dynamin-dependent maturation of bulk endocytosis restores neurotransmission following synaptic depletion. *PLoS ONE* **7**, e36913.

Oskeritzian, C. A. (2015). Mast cell plasticity and sphingosine-1-phosphate in immunity, inflammation and cancer. *Mol. Immunol.* **63**, 104-112.

Patzak, A. and Winkler, H. (1986). Exocytotic exposure and recycling of membrane antigens of chromaffin granules: ultrastructural evaluation after immunolabeling. *J. Cell Biol.* **102**, 510-515.

Pedotti, R., De Voss, J. J., Steinman, L. and Galli, S. J. (2003). Involvement of both "allergic" and "autoimmune" mechanisms in EAE, MS and other autoimmune diseases. *Trends Immunol.* **24**, 479-484.

Perrais, D., Kleppe, I. C., Taraska, J. W. and Almers, W. (2004). Recapture after exocytosis causes differential retention of protein in granules of bovine chromaffin cells. *J. Physiol.* **560**, 413-428.

Scepek, S. and Lindau, M. (1993). Focal exocytosis by eosinophils–compound exocytosis and cumulative fusion. *EMBO J.* **12**, 1811-1817.

Slutsky, B., Jarvis, D., Bibb, P., Feldberg, R. S. and Cochrane, D. E. (1987). Viability and recovery from degranulation of isolated rat peritoneal mast cells. *Exp. Cell Res.* **168**, 63-78.

Taraska, J. W., Perrais, D., Ohara-Imaizumi, M., Nagamatsu, S. and Almers, W. (2003). Secretory granules are recaptured largely intact after stimulated exocytosis in cultured endocrine cells. *Proc. Natl. Acad. Sci. USA* **100**, 2070-2075.

Tsuboi, T., McMahon, H. T. and Rutter, G. A. (2004). Mechanisms of dense core vesicle recapture following "kiss and run" ("cavicapture") exocytosis in insulin-secreting cells. *J. Biol. Chem.* **279**, 47115-47124.

Williams, R. M. and Webb, W. W. (2000). Single granule pH cycling in antigen-induced mast cell secretion. *J. Cell Sci.* **113**, 3839-3850.

Wu, W. and Wu, L.-G. (2007). Rapid bulk endocytosis and its kinetics of fission pore closure at a central synapse. *Proc. Natl. Acad. Sci. USA* **104**, 10234-10239.

Wu, Y., Ma, L., Cheley, S., Bayley, H., Cui, Q. and Chapman, E. R. (2011). Permeation of styryl dyes through nanometer-scale pores in membranes. *Biochemistry* **50**, 7493-7502.

Wu, L.-G., Hamid, E., Shin, W. and Chiang, H.-C. (2014). Exocytosis and endocytosis: modes, functions, and coupling mechanisms. *Annu. Rev. Physiol.* **76**, 301-331.

Xiang, Z., Block, M., Löfman, C. and Nilsson, G. (2001). IgE-mediated mast cell degranulation and recovery monitored by time-lapse photography. *J. Allergy Clin. Immunol.* **108**, 116-121.

Yurt, R. W., Leid, R. W. and Austen, K. F. (1977). Native heparin from rat peritoneal mast cells. *J. Biol. Chem.* **252**, 518-521.